Global Change Biology (2001) **7,** 797–815

The regional effects of CO_2 and landscape change using a coupled plant and meteorological model

JOSEPH L. EASTMAN,*,‡ MICHAEL B. COUGHENOUR† and ROGER A. PIELKE, SR.‡

**Department of Biology, University of New Mexico, Albuquerque, NM 87131, †Natural Resources Ecology Laboratory, Colorado State University, Fort Collins, CO 80523, ‡Department of Atmospheric Sciences, Colorado State University, Fort Collins, CO 80523, USA*

Abstract

A meteorological model, the Regional Atmospheric Modelling System (RAMS), and a plant model, the General Energy and Mass Transfer Model (GEMTM), are coupled in this study. The integrated modelling system was used to investigate regional weather conditions in the central grasslands of the USA for three experimental scenarios:

- **land cover is changed from current to potential vegetation;**
- **radiative forcing is changed from 1 × CO_2 to 2 × CO_2; and**
- **biological CO_2 partial pressures are doubled.**

Results indicate that the biological effect of enriched CO_2, and of land-use change exhibit dominant effects on regional meteorological and biological fields, which were observed for daily to seasonal time scales and grid to regional spatial scales. Simulated radiation impacts of 2 × CO_2 were minimal, with interactive effects between the three experimental scenarios as large as the radiational impact alone. Model results highlight the importance of including 2 × CO_2 biological effects when simulating possible future changes in regional weather.

Keywords: CO_2, feedbacks, land-use, mesoscale, radiation, regional, vegetation

Received 22 December 1999; revised version received and accepted 25 September 2000

Introduction

The role of CO_2 and/or land-use change on climate has been the focus of several research efforts (e.g. Bonan *et al*. 1992; Lyons *et al*. 1993; Claussen 1994, 1998; Dirmeyer & Shukla 1994; Foley 1994; Avissar 1995; Cutrim *et al*. 1995; Sivillo *et al*. 1997; Texier *et al*. 1997; De Ridder & Gallee 1998; Kanae *et al*. 1999; Kiang & Eltahir 1999; Li *et al*. 2000; O'Brien 2000; Wang & Eltahir 2000a; see also the review in Pielke 2001). Foley *et al*. (1998) suggest, however, that linked global and vegetation models have been limited by the consideration of only equilibrium responses of vegetation to shifting climate and the utilization of separate models that might not be physically consistent. It has also been suggested that the wide timescales at work make this an initial value problem with numerous possible outcomes (Pielke 1998; Pielke *et al*. 1999).

Recent work simulating palaeoclimate changes on the global scale (De Noblet *et al*. 1996; Claussen & Gayler 1997; Crowley & Baum 1997; Texier *et al*. 1997; Brostrom *et al*. 1998; Ganopolski *et al*. 1998) and on the regional scale in the west Africa region (Kiang & Eltahir 1999; Wang & Eltahir 2000a,b,c,d) indicate a crucial role for biospheric feedbacks on climate. Several biophysical, biogeochemical, and biogeographical parameters have been shown to have an impact on the atmosphere. These include, for example, albedo, stomatal conductance, rooting profile, fractional coverage, roughness length and displacement height, the time of planting and harvesting, vegetation phenology, and plant growth. Their effects on the atmosphere will influence, amongst other things, the diurnal temperature evolution, wind profile, turbulent transfer, Bowen ratio, precipitation, soil

*Correspondence: Joseph Eastman, Department of Atmospheric Science, Colorado State University, Fort Collins, CO 80523, USA, tel/fax +1/970-491-8293, e-mail dallas@cobra.atmos.colostate.edu

wetness and soil temperature, and evaporation. Although the relative role of radiative and stomatal conductance in a global model has been compared (Sellers *et al*. 1997), other biophysical effects, such as the effect of enriched CO_2 concentration on plant growth, have not yet been incorporated. In the Betts *et al*. (1997) evaluation of the physiological and structural feedbacks on a doubled CO_2 climate, it was found that structural changes in vegetation partially offset the physiological vegetation–climate feedbacks over the long term. It was also suggested that overall vegetation feedbacks could cause significant regional-scale effects. Previous vegetation–climate feedback simulations did not incorporate iteratively coupled model components, and therefore may not have accounted accurately for important physiological features of vegetation.

Stomatal conductance is sensitive to changes in atmospheric CO_2, with elevated CO_2 resulting in decreased stomatal conductance, and either constant or increasing photosynthesis rates. The net result is a general increase in water-use efficiency (WUE): the ratio of photosynthetic carbon gain to transpiration water loss. Clearly, this will also alter the ratio of the sensible and latent heat flux, providing another feedback on local weather conditions. In addition, changing free atmosphere CO_2 will affect growth and respiration rates (Idso 1992; Ryan *et al*. 1997). Changing the proportions of live and dead matter will produce changes in the nutrient cycling. There are other implications resulting from increasing CO_2 as outlined in Bazzaz (1990). The authors point out the following:

- C3 plants are more responsive than C4 plants to elevated CO_2.
- Photosynthesis is enhanced by CO_2 but this enhancement may decline with time.
- The response to CO_2 is more pronounced under high levels of other resources, especially water, nutrients, and light.
- Adjustment of photosynthesis during growth occurs in some species but not in others, and this adjustment may be influenced by resource availability.
- Species, even of the same community, may differ in their response to CO_2.

These points have been demonstrated in field studies (Ryan 1991; Owensby 1993). In terms of modelling efforts, these points have been generally ignored to varying degrees.

In order to investigate the effects of changing CO_2 and land-use on a regional scale, a model capable of representing the aforementioned effects is required. A modelling system that is highly mechanistic in its formulation needs to be used to ascertain the effects resulting from landscape change, radiative CO_2 forcing, and changing plant growth patterns as a consequence of enhanced CO_2 concentrations. The model must be able to simulate the nonlinear interactions between these effects at regional and local spatial scales. This mechanistic formulation was pointed out in Reynolds & Acock (1985), where they argued that plant growth models used to investigate elevated CO_2 must be mechanistic or semimechanistic in the areas that directly affect plant behaviour. This is reinforced in Chen *et al*. (1994) where much of the basis for the plant growth model used here was developed. In their work describing C4 photosynthesis, they suggest that this mechanistic approach will address the short-term effects of increasing CO_2, as well as the long-term effects resulting from plant acclimation to rising CO_2.

Photosynthetic acclimation to elevated CO_2, as pointed out by Bazzaz (1990), is species- or ecosystem-dependent. In nitrogen-poor environments, acclimation is a benefit to the plant because it needs to conserve the scarce resource. Earlier studies generally employed potted plants in their experimental design, but Eamus (1996) points out that acclimation may not be as prevalent when the roots are unconstrained. In Bryant *et al*. (1998) down-regulation was observed, yet the net rates of photosynthesis were still enhanced. In this same study, it was found that two forbs had actually reversed their decrease in rubisco activity and did not show evidence of down-regulation. In the present paper, the problem of tackling acclimation and subsequent down-regulation is not addressed by this modelling system owing to the complexity and existing lack of understanding of this issue.

Modelling tools

The meteorological model used in this investigation is the Regional Atmospheric Modelling System (RAMS). RAMS is a 3D model that employs fundamental equations of fluid dynamics. It was further modified (Liston & Pielke 2000) for longer integrations and is named ClimRAMS. ClimRAMS, a mesoscale model, has several additions to RAMS that make it desirable for assessing regional climate effects. Some of the main features of the 3D atmospheric model include:

- variable initialization and 3D nudging; 3D nudging adds a time-scale dependent prognostic term to force model-simulated quantities like wind, temperature, and moisture, towards observations at the outer boundaries (within 5 gridpoints of the lateral boundary for these simulations);
- dump bucket precipitation (Cotton *et al*. 1995)—this scheme evaluates the saturation levels in the atmosphere, and assuming an efficiency for precipitation, removes the excess moisture as precipitation;
- Kuo cumulus convection parameterization (Kuo & Raymond 1980); this is a simple parameterization that simulates cumulus convection and is triggered by

exceeding a threshold of vertical motion at the model-simulated cloud base;
- longwave and shortwave radiative fluxes (Mahrer & Pielke 1977)—this scheme is rather simple, and does not account for attenuation of shortwave radiation by clouds;
- multilevel soil model to simulate variable soil temperature and moisture (Tremback & Kessler 1985);
- additional subroutines to simulate grid-scale snow accumulation, snow melt, and their effects on surface hydrology and surface energy budgets.

ClimRAMS advects and diffuses the atmospheric CO_2 and simulates diurnal, as well as seasonal changes in CO_2 that are representative of observational studies, such as Bazzaz & Williams (1991). The CO_2 concentrations resulting from these calculations can be used in both biological and radiative calculations, or for each one separately, leaving the other constant.

ClimRAMS has been successfully linked to the General Energy and Mass Transfer Model (GEMTM; Chen *et al*. 1994). The ClimRAMS and GEMTM models are physically consistent in their formulations, as both are based on similar theory for prognosing surface energy budgets (Eastman 1999). The version of GEMTM used in this study contains the following:
- explicit C3 (Farquhar *et al*. 1980) and C4 (Collatz *et al*. 1992; Chen & Coughenour 1994) photosynthesis;
- allocation, respiration, plant growth and mortality rates based on temperature and moisture relationships;
- spatially explicit root model for effluence and uptake, including branching and lengthening algorithms (Chen & Lieth 1992, 1993);
- multilevel canopy radiation model for prediction of diffuse and direct radiation (Goudriaan 1977; Chen 1983);
- variable biomass initialization;
- unlimited species types.

Both models are interfaced on a common timestep of 90 s. The meteorological model calculates several soil and surface related quantities, such as soil moisture and temperature, as well as water and heat fluxes. In the calculation of soil moisture in the root zone, a dynamically changing root resistance model is employed. The model allows water to be absorbed and released from the roots. It is assumed that the transpiration rate is equal to the soil water uptake for calculations of the plant water potential at the base of the xylem. These calculations involve several surface-vegetation related quantities including albedo, fractional coverage, Leaf Area Index (LAI, $m^2\ m^{-2}$), and roughness length, with the latter three updated daily. Surface radiation, soil temperature, and soil moisture parameters are in turn employed for algorithms used to calculate direct and diffuse radiation, with a separate photosynthesis calculation performed for direct and diffuse photosynthetically active radiation (PAR). The model calculates respiration, mortality, growth rates, and allocation to roots, shoots, leaves, and seeds, using temperature and moisture relations. At the end of the modelling day, 0 GMT here, the plant model updates root characteristics. This involves allocation to branching and lengthening and subsequent root weighted density according to the available net photosynthate. The allocation is based on water and temperature stress at a given root level.

The updated stomatal conductance, calculated according to Ball *et al*. (1987), LAI, roughness length, and fractional coverage are then returned to the meteorological model. These quantities are then used in similarity theory calculations in ClimRAMS to modify the surface heat and moisture flux. The fractional coverage is used to weight the net heat and moisture flux due to bare and shaded soil, water, and vegetation.

Initialization

The different components of the modelling system require several datasets in order to initialize simulations. The domain used is shown with the natural and current vegetation distributions (Fig. 1a,b). Horizontal grid spacing is 50 km. For the vertical coordinates, an initial increment of 100 m is used at the surface, which is then slowly increased to 1.5 km near the top of the model. There are 30 points in the E–W direction, 26 points in the N–S direction, and 20 points in the vertical. Topography was initialized using the USGS 30 s dataset.

All simulations were integrated for 210 days over the growing season, beginning on 1 April 1989. In order to simulate the 1989 growing season, the model uses a Newtonian relaxation method at the outer 3 grid points of the domain. Newtonian relaxation adds a tendency term to the prognosed quantity that drives it towards the observations from the NCEP reanalysis product (Kalnay *et al*. 1996). The reanalysis product was used to create the initial fields, as well as the lateral boundary conditions. The data are processed through an isentropic analysis package, which is interpolated to the ClimRAMS grid.

The Vegetation Mapping and Analysis Project (VEMAP, Kittel *et al*. 1995) provided the vegetation distribution for the current and potential landscapes (Küchler 1964; Küchler 1975). In order to set the above- and belowground biomass fields, the Advanced Very High Resolution Radiometer (AVHRR) derived Normalized Difference Vegetation Index (NDVI) product was used to calculate spatially explicit LAI using a separate algorithm for woody and herbaceous vegetation (Asrar *et al*. 1984; Nemani & Running 1989). Leaf biomass was in turn determined from a specific leaf area consist-

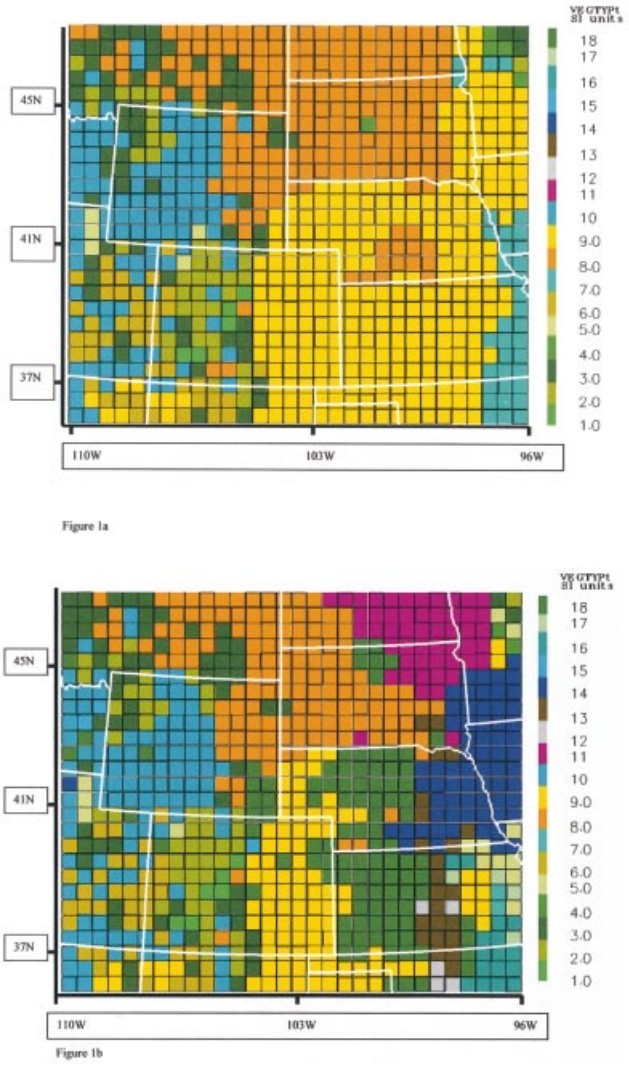

Fig. 1 (a) Modelling domain and natural vegetation distribution. (b) modelling domain and current vegetation distribution. Classes represent: 1, tundra; 2, subalpine; 3, temperate conifer; 4, temperate deciduous; 5, temperate xeromorphic; 6, temperate coniferous xeromorphic; 7, savanna and deciduous; 8, C3 shortgrass; 9, C4 tall grass; 10, temperate arid shrub; 11, spring wheat/small grass; 12, small grains; 13, winter wheat; 14, corn; 15, irrigated crop; 16, deciduous forest crop; 17, subtropical mixed forest; and 18, grassland and grain.

ent with the biome type. Shoot biomass was determined through a literature survey of typical leaf and shoot biomass observed for different vegetation classes. Finally, a plant-specific root-to-shoot ratio was used to determine the belowground biomass for herbaceous vegetation. In the case of woody vegetation, root biomass was determined using the shoot biomass corresponding to the yearly maximum LAI determined from the AVHRR–NDVI data.

Table 1 Summary of the 8 simulations performed and the symbols used to refer to them

Simulation symbol	Vegetation	CO_2 radiation	CO_2 biology
f_0	Current	1×	1×
f_1	Natural	1×	1×
f_2	Current	2×	1×
f_3	Current	1×	2×
f_{12}	Natural	2×	1×
f_{13}	Natural	1×	2×
f_{23}	Current	2×	2×
f_{123}	Natural	2×	2×

A spatially variable objective analysis was employed to initialize the soil model. The soil class data are directly read from the STATSGO soils dataset (U.S. Department of Agriculture 1994). Soil textural class is assumed uniform within the vertical column. Data used to variably initialize the soil moisture and temperature profiles are a product of the ECMWF/TOGA Advanced Operational Analysis Data. The soil wetness and temperature are based on this product following the work of Mintz & Serafini (1981). The surface soil climatological moisture corresponds to a layer from the surface to a depth of 7.2 cm. The deep-layer climatological soil moisture and temperature values are derived for a layer from 7.2 cm to a depth of 42 cm. Soil data are defined spatially on a 1° × 1° grid, while the temporal resolution is a one-month averaged field. The initial soil temperature and moisture fields are defined by linear interpolation between the 42-cm-deep climatology soil temperature and moisture, and the RAMS objectively analysed surface temperature fields. Soil grid points below the 42 cm depth are set to the 42 cm value. The bottom soil layer, at 2 m below ground, then serves as a nudging boundary condition and is temporally interpolated between monthly values of the climatological dataset for moisture only.

Hypothesis and experimental design

In the introduction, the various interactions for CO_2 and vegetation were discussed briefly. Using a mechanistic model, the various perturbation experiments (which we will call factors), can be quantified individually through a separation technique designed by Stein & Alpert (1993). This separation also enables the examination of the nonlinear interactions between the factors. This study examines the contributions of vegetation change (potential and current), 1× and 2 × CO_2 radiative forcing, and 1× and 2 × CO_2 concentrations felt only by the biota (called CO_2 biology from here on). It also examines the

Table 2 Description of the difference fields and their meaning

Difference	Contribution resulting from
$f_1 - f_0$	natural vegetation
$f_2 - f_0$	$2 \times CO_2$ radiation
$f_3 - f_0$	$2 \times CO_2$ biology
$f_{12} - (f_1 + f_2) + f_0$	the interaction of natural vegetation and $2 \times CO_2$ radiation
$f_{13} - (f_1 + f_3) + f_0$	the interaction of natural vegetation and $2 \times CO_2$ biology
$f_{23} - (f_2 + f_3) + f_0$	the interaction of $2 \times CO_2$ radiation and $2 \times CO_2$ biology
$f_{123} + (f_1 + f_2 + f_3) - (f_{12} + f_{13}\ f_{23}) - f_0$	the interaction of natural vegetation, $2 \times CO_2$ radiation, and $2 \times CO_2$ biology

various interactive combinations of these factors. The eight simulations needed to perform the analysis are outlined in Table 1, and the difference fields of each factor contribution are shown in Table 2.

Significant differences in the domain-averaged prognosed meteorological and biological fields between the control simulation and perturbation simulations are examined when:

- land cover is changed from current to potential vegetation;
- radiative forcing is changed from $1 \times CO_2$ to $2 \times CO_2$; and
- biological CO_2 concentrations are doubled.

The results are examined through temporal domain averages, domain- and temporal-averaged means and biases, and spatial time series at individual gridpoints. The analysis is performed for daily updated variables and 2-h averaged data. The Kolmogorov–Smirnoff (KS) test (Anderson & Darling 1952) is used to determine whether significant differences are present in the cumulative distribution function.

Results

Validation

Meteorology. The control simulation, f_0, was initially compared against observed data from standard meteorological stations, to quantify the ability of the simulation in capturing major trends in regional weather patterns. The meteorologically observed data were produced by objectively analysing surface station data for the ClimRAMS model grid. The meteorological variables tested were maximum daily temperature, minimum daily temperature, and daily precipitation. Spatially explicit plots were created from a comparison of the temporal series at each gridpoint for the modelled and observed variable.

A spatially explicit correlation coefficient, *r*, and bias were calculated for the temperature fields and are shown in Figs 2(a)–(b) and 3(a)–(b), respectively. Modelled temperature fields exhibit an acceptable degree of correlation with the model for both maximum and minimum daily temperature, with an *r*-value ranging from 0.72 to 0.92. There is one isolated area in the south-east portion of the domain that exhibits a relative minimum in correlation, although the values are still higher than 0.7. This is likely a consequence of its distance from the inflow boundaries, because the flow is from west or north-west to the east and south-east portions of the domain. This implies that this area would receive the least amount of information from the lateral boundaries.

Fig. 3(a)–(b) presents the spatially explicit plots for the bias in the indicated variable. The warmest maximum temperature bias is indicated in the area where the lowest correlation was found. The magnitudes are around 2–3 °C throughout the area. There also appears to be a significant cool bias in the western portions of the domain. These likely result from the influence of topography, which is not well resolved with the 50-km grid.

Domain-averaged correlation, bias, and KS statistic were calculated for temperature fields. These are summarized in Table 3. The KS statistic indicates that neither the maximum nor minimum daily temperature distributions are significantly different between the model and observations at the $\alpha = 0.05$ significance level. A value of 1.0 would indicate a perfect match between the datasets. The correlation coefficients are also relatively high on a domain-averaged scale. Finally, the biases indicate that the domain-averaged maximum daily temperature is undersimulated by nearly a degree, while the domain-averaged minimum daily temperature is undersimulated by just over a tenth of a degree. These numbers indicate that the model has captured the regional weather patterns observed during the 1989 growing season. Such validation experiments show that the precipitation was considerably more difficult than temperature to predict. Simulated precipitation was found to be about 60% of the observed values, except during large-scale synoptic events in the spring and fall, where the tendency was to overpredict.

A plot of the domain-averaged precipitation is displayed in Fig. 4. Validation experiments indicate that the present model does a reasonable job of capturing the temporal progression of the domain-averaged rainfall. Summer period precipitation predictions appear to be consistently undersimulated.

Biological. In order to help validate plant model predictions, AVHRR–NDVI-derived LAI was compared to the simulated fields using a 10-d averaged temporal

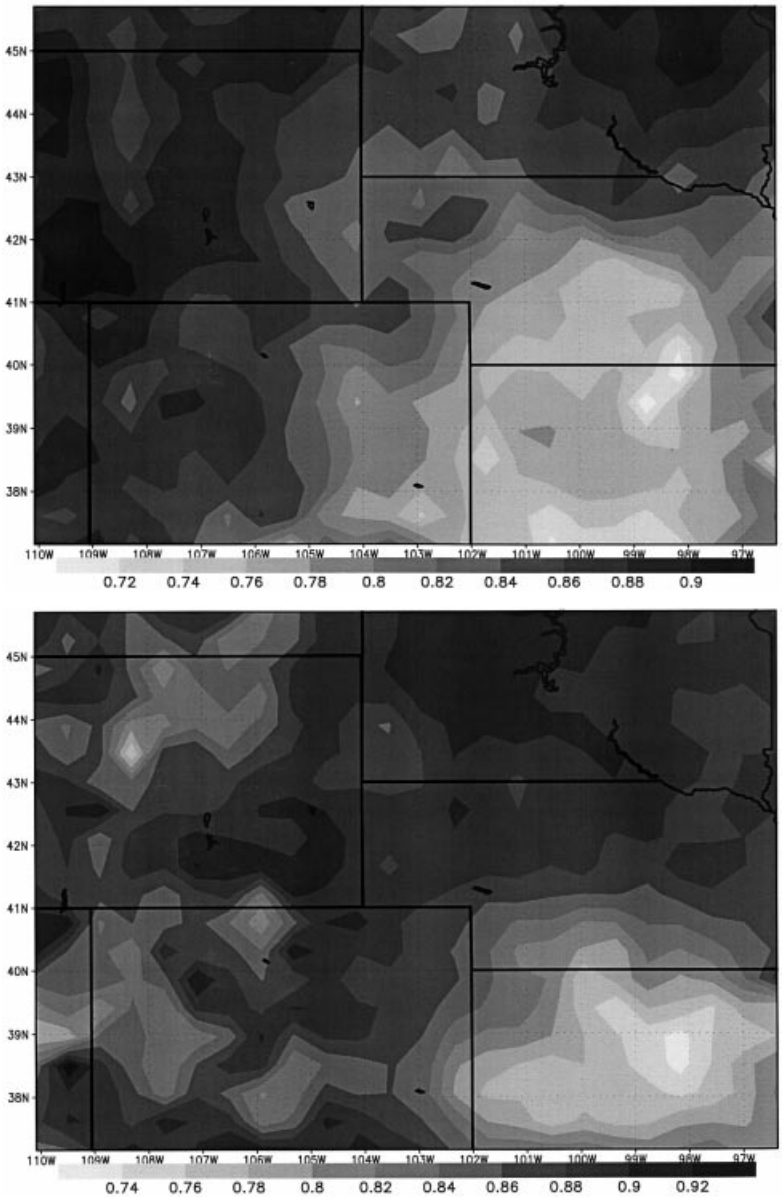

Fig. 2 Pearson's correlation coefficient between the observations and the model for (a) maximum daily temperature, and (b) minimum daily temperature.

series from 1 April 1989 to 31 October 1989. The spatially explicit correlation coefficient is displayed in Fig. 5. The figure indicates that most of the domain has correlation coefficients greater than 0.6, with significant portions above 0.8. In the eastern portion of the domain there are values less than 0.4, with negative values over the deciduous forest/mixed crop cells. The mixed class with herbaceous and woody vegetation makes the prediction of LAI considerably more difficult because of the substantial differences in biophysical parameters. A patch-dependent scheme might ameliorate some of this difficulty, as a given patch would contain only one set of parameters specific to woody or herbaceous vegetation.

Figure 6 displays the seasonally-averaged bias in LAI. The eastern half of the domain indicates a bias between ± 0.1 m^2 m^{-2}. Over the western portion of the domain, where LAI can reach 10, the range is ± 0.3 m^2 m^{-2}. These values are a smaller percentage of total LAI when compared to the plains, where LAI is commonly around 1.0. Overall, the model exhibits agreement with observations in predicting the seasonal evolution of LAI.

Domain-averaged factor effects

Having demonstrated that the coupled model has captured the patterns in the meteorological and biological fields, an evaluation can be made of the effects of CO_2

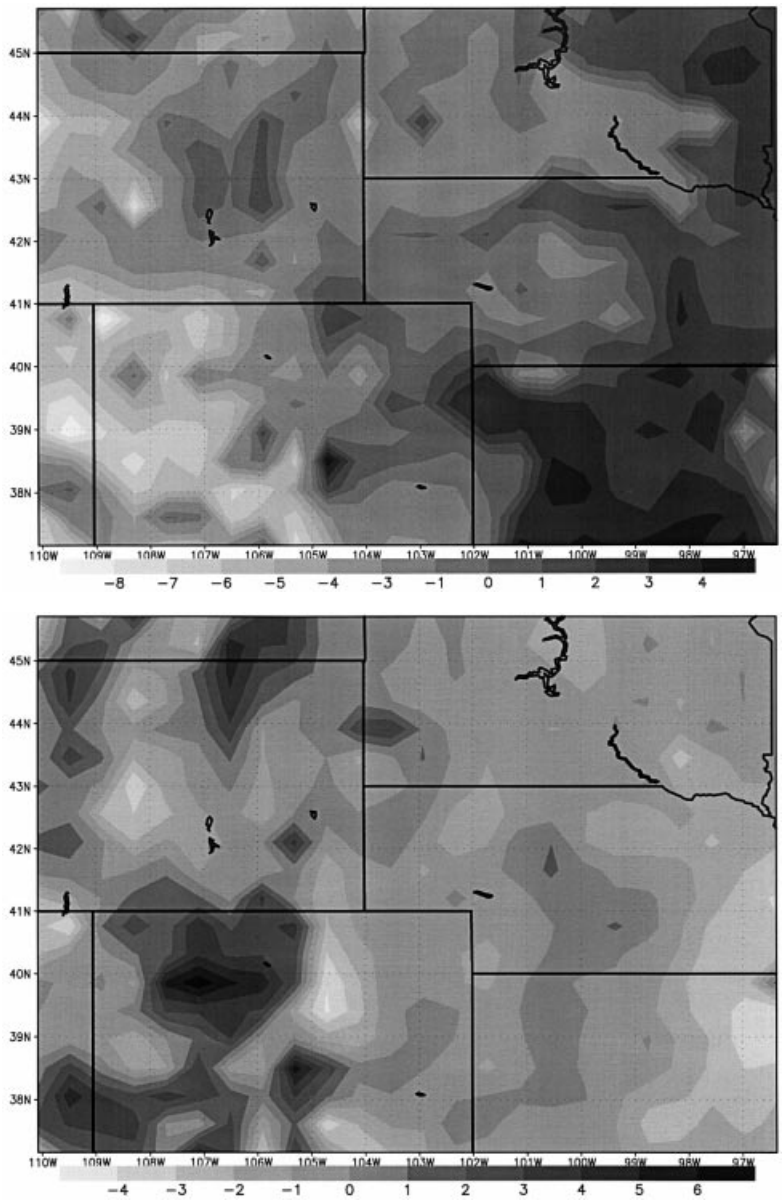

Fig. 3 Bias (°C) between the model and observations for (a) maximum daily temperature; and (b) minimum daily temperature.

atmospheric concentrations and land-use change on the simulation of seasonal weather. Starting with domain-averaged means and standard deviation, σ, for the variables used in the validation, additional variables are also analysed in this section. Their symbols and definitions are indicated in Table 4.

Maximum daily temperature. The data in Table 5 show the mean and standard deviation for selected variables. The control simulation values are displayed for comparison to the factor contributions indicated under the columns for natural vegetation, $2 \times CO_2$ radiation, and $2 \times CO_2$ biology.

It is clear from the data in Table 5 that the natural vegetation has the largest effect on the maximum daily temperature, with a mean cooling contribution of 1.191 °C, and a standard deviation of 1.770 °C. The contribution to maximum temperature is small for $2 \times CO_2$ radiation, with a mean of 0.014 °C, while the $2 \times CO_2$ biology indicates a relatively large cooling contribution of 0.747 °C. The cooling effects for natural vegetation and $2 \times CO_2$ biology are associated with increased fractional vegetation coverage in both simulations resulting in increased transpiration of water vapour. In the $2 \times CO_2$ biology treatment reduced transpiration per stoma was more than compensated

for by the greater coverage of vegetation. In the current landscape, fields are barren for significant portions of the spring and in the autumn during harvesting, which would clearly lead to higher daytime temperatures. The contribution from $2 \times CO_2$ biology is an integrative effect that operates for the entire simulation period.

The contributions of the factors and their interactions are displayed graphically in Fig. 7. The interactions represent the nonlinear response resulting from the interaction of the two factors, and do not contain the contribution due to the factors themselves. In this way, their interpretation is somewhat difficult to describe with physical mechanisms, and is generally smaller in amplitude than the dominant factors by themselves. In terms of interactions, the combination of natural vegetation and $2 \times CO_2$ biology produces the largest contribution. It might be expected to be larger, given the results for $2 \times CO_2$ biology by itself. However, in the natural landscape there is substantially more C4 tall grass

Table 3 Statistical quantities for domain-averaged maximum and minimum daily temperatures

Variable	*r*	KS statistic	Bias
Maximum daily temperature	0.8875	0.1122	– 0.9790
Minimum daily temperature	0.9057	0.7112	– 0.1579

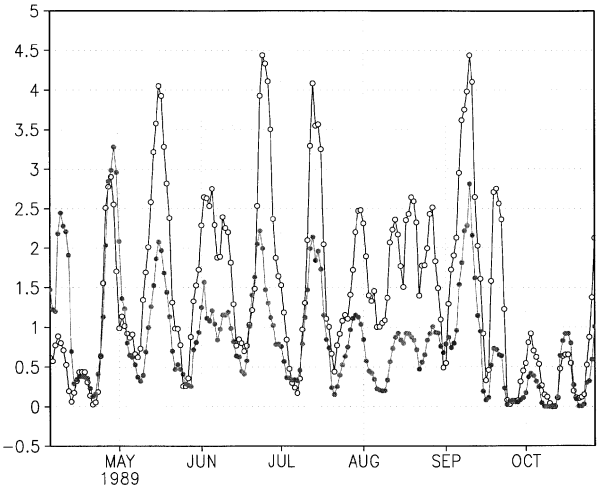

Fig. 4 Domain-averaged daily precipitation for the model (grey line) and observations black line). A 3-day sliding window was applied to smooth the data.

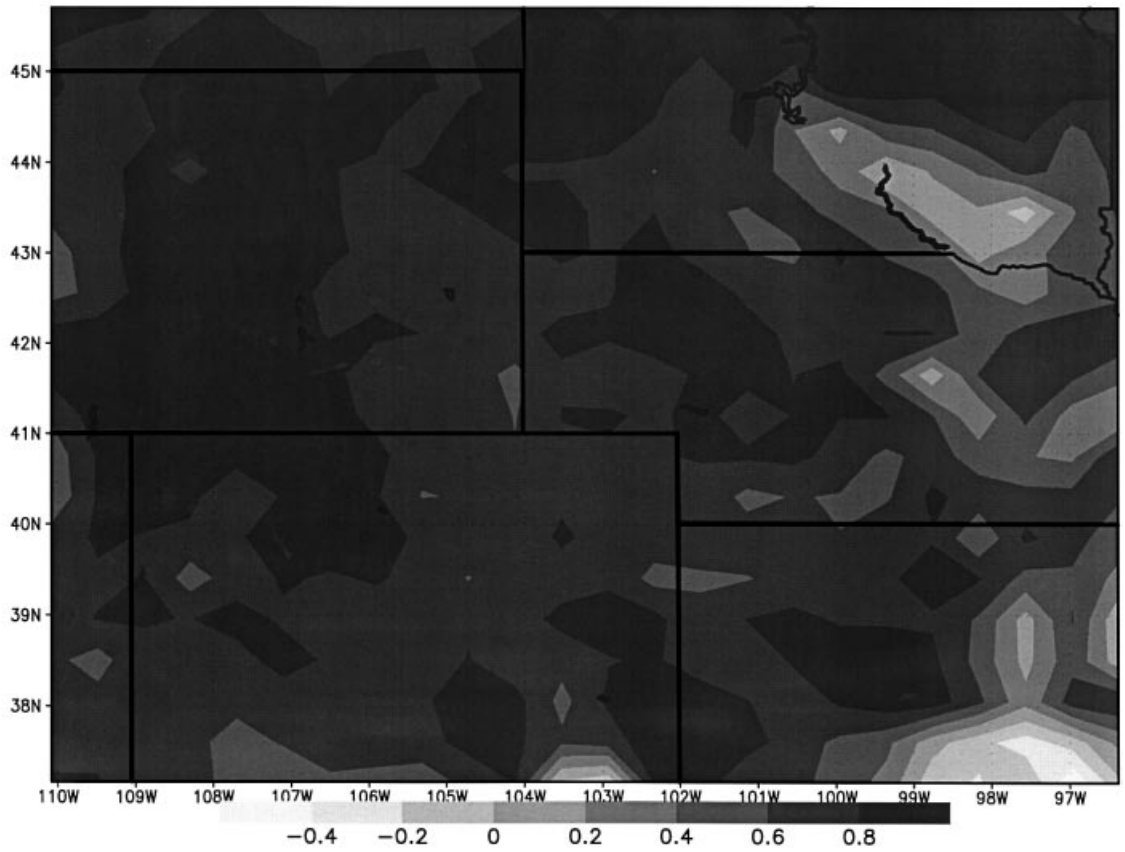

Fig. 5 Correlation of observed and modelled LAI (m^2 m^{-2}).

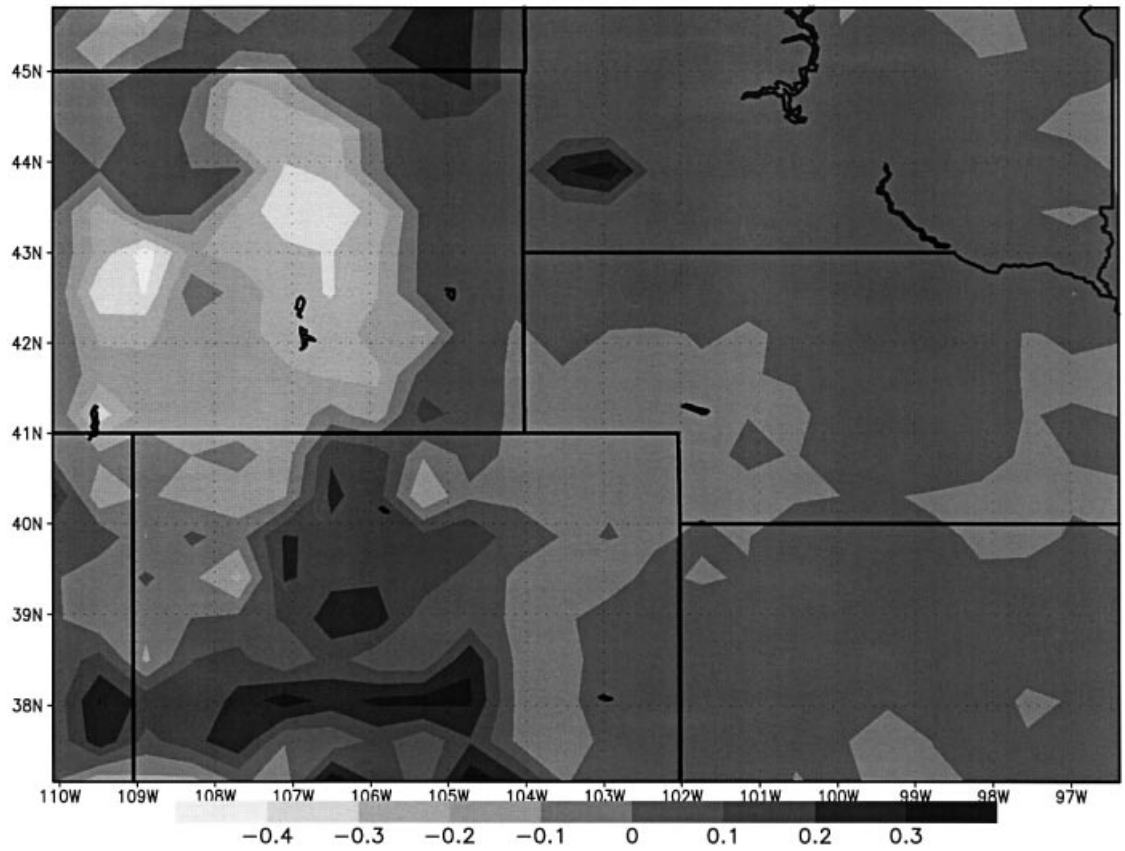

Fig. 6 Seasonally averaged bias in LAI (m^2 m^{-2}) between the model and observations.

Table 4 Variables included in the domain-averaged analysis, and their description

Variable	Description
TMAX	Maximum daily temperature
TMIN	Minimum daily temperature
PPT	Daily accumulated precipitation
ACCUMALL	Total accumulated precipitation
LAI	Leaf Area Index
DLAI	Daily LAI change
WLF	Leaf biomass
WSH	Shoot biomass
WR	Root biomass
TRANS	Daily net transpiration
SUMALL	Total accumulated carbon

present. Because C4-plant anatomy permits build-up of CO_2 near the site of carboxylation, photosynthesis in C4-plants is minimally influenced by changes in atmospheric CO_2.

Minimum daily temperature. The means for minimum daily temperature contributions indicate slight cooling for natural vegetation; however, the standard deviation is 4 times this magnitude, which indicates that spatial plots show large areas of both warming and cooling. The radiative effect is roughly a tenth of a degree, and is a relatively consistent contribution as indicated by its small standard deviation. The $2 \times CO_2$ biology treatment indicates the strongest warming, with a mean of 0.261 °C. At night, the greater vegetation coverage leads to higher atmospheric water vapour content that elevates the dewpoint temperature, thus leading to warmer minimum temperatures. The interaction of natural vegetation and $2 \times CO_2$ biology is nearly equal to the contribution of $2 \times CO_2$ radiation by itself. The rest of the interactions are quite small relative to the interaction of the natural vegetation and $2 \times CO_2$ biology treatment.

Precipitation. The analysis of daily precipitation suggests that the enhanced biomass has decreased precipitation and appears to offset any elevated transpiration resulting from increased biomass, which would imply that convective temperatures are not being reached as frequently. The peak of convective precipitation occurs in the middle summer months, and

Table 5 Domain and seasonally-averaged mean and standard deviation for the control simulation, and mean contributions and standard deviation of contributions owing to natural vegetation, 2 × CO_2 radiation, and 2 × CO_2 biology

	Current Vegetation 1 × CO_2		Natural Vegetation		2 × CO_2 radiation		2 × CO_2 biology	
Variable	Mean	σ	Mean	σ	Mean	σ	mean	σ
TMAX (°C)	23.13	4.52	– 1.191	1.77	0.014	0.159	– 0.747	0.639
TMIN (°C)	7.299	2.78	– 0.017	0.531	0.097	0.041	0.261	0.365
PPT (mm)	0.889	0.34	– 0.035	0.088	0.008	0.011	– 0.046	0.030
LAI	2.663	3.402	0.198	0.783	0.001	0.071	0.578	0.621

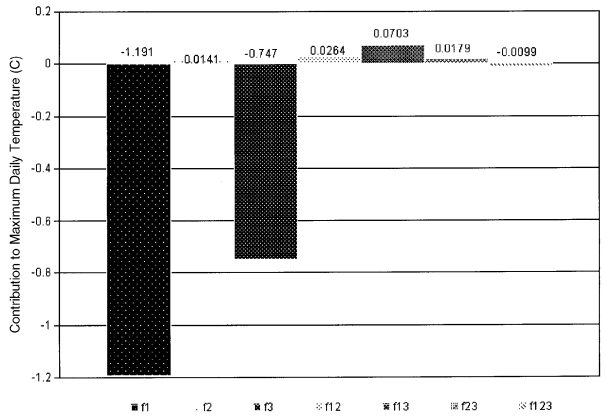

Fig. 7 The seasonal domain-averaged contributions to maximum daily temperature owing to: f_1, natural vegetation; f_2, 2 × CO_2 radiation; f_3, 2 × CO_2 biology; f_{12}, interaction of natural vegetation and 2 × CO_2 radiation; f_{13}, interaction of natural vegetation and 2 × CO_2 biology; f_{23}, interaction of 2 × CO_2 for radiation and biology; f_{123}, the interaction of all three factors.

plots of domain-averaged precipitation (not shown) indicate that the deficit was a peak during this time of the year. The 2 × CO_2 radiation contribution implies a relatively small positive input, consistent with slight increases in the temperature fields. The factor interactions were found to exhibit minor contributions to the domain-averaged daily precipitation.

Factor effects on LAI

The results displayed in Fig. 9 show the domain-averaged contributions to LAI owing to the various factors and their interactions. It is evident from the data in Fig. 9 that the effect of 2 × CO_2 biology on the natural vegetation is less than the effect on the C3-dominated current landscape. Simulations of C4 and C3 grasses for the natural landscape shows that biomass was increased by 17% for the C4 grass, while biomass of C3 grasses was increased by more than double this amount. The meteorological feedback with the different landscapes also contributed to these differences.

Temporal analysis of factor effects

A KS test between the control simulation and factor simulations for their cumulative distribution functions was performed. A significant difference of 0.05 corresponds to a temporal shift. The results for the variables listed in Table 4 are shown in Table 6. The results in the Table show that the natural vegetation and 2 × CO_2 biology have significant impacts on the cumulative distribution function. The test statistics for 2 × CO_2 radiation indicate only one significant difference (in the root biomass). The test statistics for natural vegetation indicates significant contributions to the maximum daily temperature, while other factors do not; which is consistent with the different phenology for natural and current landscapes, indicative of crop planting and harvesting and their effects on the surface energy budget. This is also supported by the test statistic for leaf and shoot biomass.

The 2 × CO_2 biology treatment has produced a temporal shift in allocation, as suggested by the significant difference for shoot biomass, while the leaves appear to be unaffected. Finally, both the natural vegetation and 2 × CO_2 biology exhibit temporal shifts in the accumulated precipitation. As shown earlier, the effects are likely the consequence of an alteration of the surface energy budget owing to changes in the biomass and transpiration rates.

Factor effects on the diurnal cycle. Thus far, emphasis has been given to the seasonally averaged effects on daily variables. Given these results, it would be intuitive to expect effects on the diurnal cycle due to these factors. A list of 2- h averaged variables is shown in Table 7. A KS test statistic was computed for each of the variables at 0, 6, 12, and 18 GMT to discern any trend in the diurnal cycle due to the factors. An $\alpha = 0.05$ significance level was used. Instead of showing the

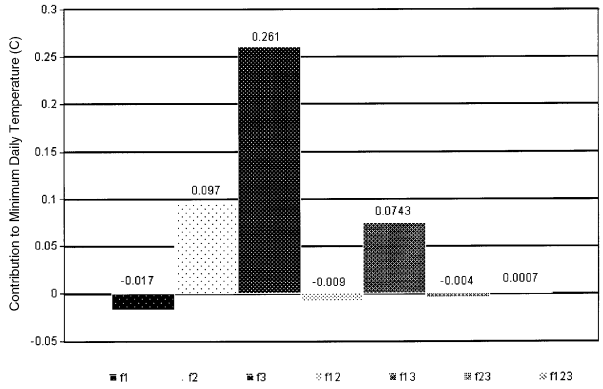

Fig. 8 Same as Fig. 7 except for minimum daily temperature contribution.

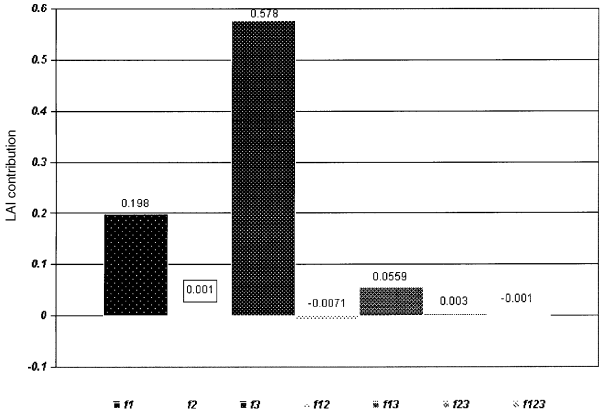

Fig. 9 Same as Fig. 7 except for LAI (m^2 m^{-2}).

results for each variable individually, the number of variables with significant differences is displayed in Fig. 10. One can see from these data that there is a strong diurnal trend for the natural vegetation simulation, which is likely the result of different temporal evolution in the underlying vegetation, and is concentrated over the areas of crops, because the western portions of the domain have undergone minor changes. The $2 \times CO_2$ biology treatment indicates no apparent diurnal changes, while the $2 \times CO_2$ radiation test statistics suggest no variables with a significant difference in the cumulative distribution function. When a *t*-test was applied to test for significant differences in means, the 18 and 0 GMT results suggested strong significant differences for the natural vegetation and $2 \times CO_2$ biology simulations, with the natural vegetation displaying the most differences. As in the KS test, the $2 \times CO_2$ radiation showed no significant differences.

Table 6 KS statistic for comparison of the cumulative distribution of the control simulation and the listed factor. Values significant at the $\alpha = 0.05$ are shaded grey

	KS statistic		
Variable	Natural vegetation	$2 \times CO_2$ radiation	$2 \times CO_2$ biology
TMAX	**0.298E – 01**	0.100E + 01	0.393E + 00
TMIN	0.100E + 01	0.100E + 01	0.923E + 00
ACCUMALL	**0.864E – 02**	0.792E + 00	**0.618E – 02**
LAI	**0.505E – 19**	0.987E + 00	**0.222E – 41**
DLAI	**0.879E – 01**	0.100E + 01	**0.307E – 02**
WL	**0.108E – 30**	0.987E + 00	0.100E + 01
WSH	**0.174E – 04**	0.100E + 01	**0.741E – 20**
WR	0.100E + 01	**0.618E – 02**	0.100E + 01
TRAN	0.671E – 03	0.100E + 01	0.465E + 00
SUMALL	0.199E – 04	0.100E + 01	**0.104E – 20**

Spatial analysis of factor effects

In order to examine the spatial nature of some of the variables, a *t*-test and KS test statistic can be computed, using a temporal series at each gridpoint, to test whether the control and factor simulations have significantly different means or cumulative distributions, respectively. This information is summarized in Table 8.

Under the columns for natural vegetation, a surprising result emerges. Keeping in mind that 41.3% of the gridpoints change vegetation class when comparing current and natural vegetation, note the higher percentage of cells exhibiting significant differences for both the *t*- and KS tests. In the case of the KS test for daily precipitation, the percentage is nearly double the vegetation change percentage. The *t*-test does not indicate that high of percentage. Clearly, there has been a strong temporal shift in precipitation events that is nearly domain-wide, while the magnitude of events has changed to a lesser degree.

In the case of several of the biological variables, the statistics in Table 8 suggest that there are nearly 25% more cells with significant differences than those with vegetation change. This might best be described as a 'biological teleconnection' similar to El Niño's global impacts. In this case, there is a potential regional response, where the effects of changing vegetation have been communicated to other portions of the domain through the atmospheric transfer of water, heat, and momentum. An example of this is displayed in Fig. 11. This figure displays the KS test results for shoot biomass. The lighter grey areas indicate no significance, while the darker grey areas represent significant differences at the $\alpha = 0.05$ value. The contour lines denote the boundary

between altered and unaltered vegetation. The figure indicates that the area with significant differences is clearly larger than the area of vegetation change. Large portions of the natural shortgrass are exhibiting differences despite being unchanged. Many of the areas showing significant differences are distant from the change. It is also apparent that some areas where change has occurred indicate no significant differences. These results suggest that regional response is not a simple linear response, and that changing one area's biota can affect distant areas.

Examining the data in other columns of Table 8, it is clear that the $2 \times CO_2$ radiation has little effect on anything, except the distribution of rainfall and, to a limited degree, biological variables. In the case of $2 \times CO_2$ biology, the effect on precipitation and the biota is large for both the distributions and means. The small percentage with significant differences for transpiration implies that the $2 \times CO_2$ biology has reduced stomatal conductance and subsequent transpiration, which appears to be offset by the increased leaf biomass for roughly 80% of the domain. As was found for the landscape change and $2 \times CO_2$ radiation, the $2 \times CO_2$ biology effects are large for precipitation, which suggests that precipitation is a highly nonlinear process that responds strongly to small perturbations.

It has been shown from the data that $2 \times CO_2$ radiation exhibits a relatively minor role in the coupled biological and atmospheric system. In fact, interactions display a larger effect on limited variables. With this in mind, natural vegetation and $2 \times CO_2$ biology monthly averaged contributions will be concentrated upon in the last set of figures.

Table 7 Symbols and description of 2- h averaged variables

Variable	Description
QFZ	Latent heat flux
TFZ	Sensible heat flux
WFZ	Momentum flux
SOIL1	Soil temperature at 1.0 m
SOIL2	Surface soil moisture
SWPAVG	Soil water potential in the root zone
SWPTOP	Soil water potential in the top 0.25 m
PLWP	Plant water potential at the xylem base
GS	Stomatal conductance
AN	Assimilation rate
RESS	Soil respiration
CO2FLX	CO_2 flux at the surface
CO2SFC	CO_2 concentration at the surface
RHAIR	Relative humidity at 2.0 m

Factor effects on monthly-averaged maximum daily temperature

In the first series of plots (Fig. 12a), the average maximum daily temperature fields for the natural minus the current vegetation simulations are displayed. The fields are one-month averages for maximum daily temperature. In both simulations, $1 \times CO_2$ radiation and biology were used. The plot in panel (i) shows the seasonally-averaged difference. The effects of the crops in the eastern plains are readily apparent. The differences suggest that under current vegetation, this area exhibits warming between 1

Table 8 Percentage of grid points significantly different for means and cumulative distributions at $\alpha = 0.05$ between the control simulation and natural vegetation, $2 \times CO_2$ radiation, and $2 \times CO_2$ biology simulations. Values in bold indicate the highest percentage of any factor. Values underlined indicate a percentage higher than the total percentage of grid cells changed between current and natural vegetation. Bold and underlined values meet both criteria

	Natural vegetation		$2 \times CO_2$ radiation		$2 \times CO_2$ biology	
Variable	% cells t test	% cells KS test	% cells t test	% cells KS test	% cells t test	% cells KS test
TMAX	**39.8**	**40.6**	0.0	0.0	14.6	18.1
TMIN	**3.1**	**3.1**	0.0	0.0	0.0	0.6
ACCUMALL	**16.9**	78.1	0.4	49.0	11.7	**89.6**
PPT	**6.2**	81.5	0.0	77.3	0.0	**84.2**
VFRAC	52.1	24.2	4.8	24.2	**86.7**	**58.8**
LAI	50.8	25.8	6.0	15.6	**97.5**	**66.7**
DLAI	37.5	50.0	1.3	6.9	**40.0**	**91.5**
WL	50.6	25.6	6.0	15.6	**97.5**	**66.7**
WSH	46.3	57.9	6.0	16.0	**89.4**	**81.7**
WR	49.8	27.3	5.0	25.2	**77.7**	**57.5**
TRAN	**45.6**	**43.5**	1.5	1.5	20.0	20.8
SUMALL	52.7	35.5	8.3	21.7	**99.8**	**66.0**

and 5 °C over most of the region. To the west, where little change in land-use has occurred, the effects appear to be minimal, with warm and cool spots highly localized. There is a general strengthening in the signal over the plains moving from April to June. At the same time, the western portions of the spatial plots suggest that the areal extent of areas experiencing cooling is decreasing.

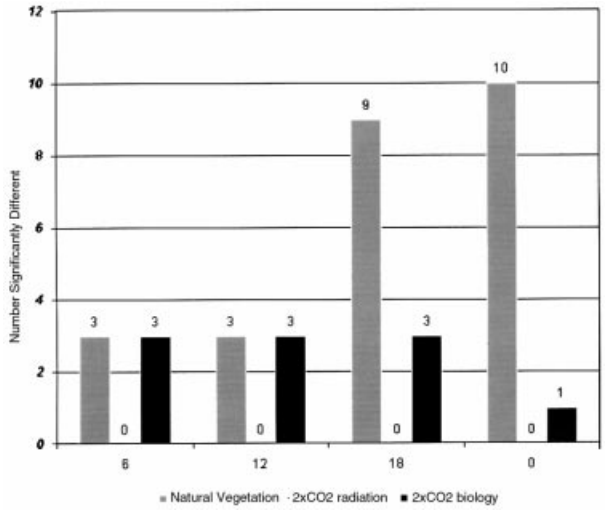

Fig. 10 The number of significant differences for the KS test vs. time of day for the factor contribution (indicated by the legend). The variables are defined in Table 7.

The rest of the temporal series is presented in Fig. 12(b), and corresponds to July–October. The series exhibits a strengthening of warming over agricultural areas up to August, at which time the signal begins to dissipate. The western portion of the domain has continued to warm slightly until August, at which time it oscillates from cool to warm to cool over the 3-month period, indicating a seasonal effect.

Overall, the strongest signal appears over areas of land-use change. There are also indications that regions not experiencing the change undergo a seasonal evolution that switches between cooling and warming. As in the analysis examining cell percentages, the biological teleconnection is operating at different temporal scales that are not evident in the seasonally-averaged analysis.

The simulation data in Fig. 13(a,b) show a similar series of plots for the natural minus the current vegetation simulations, the only difference being that the

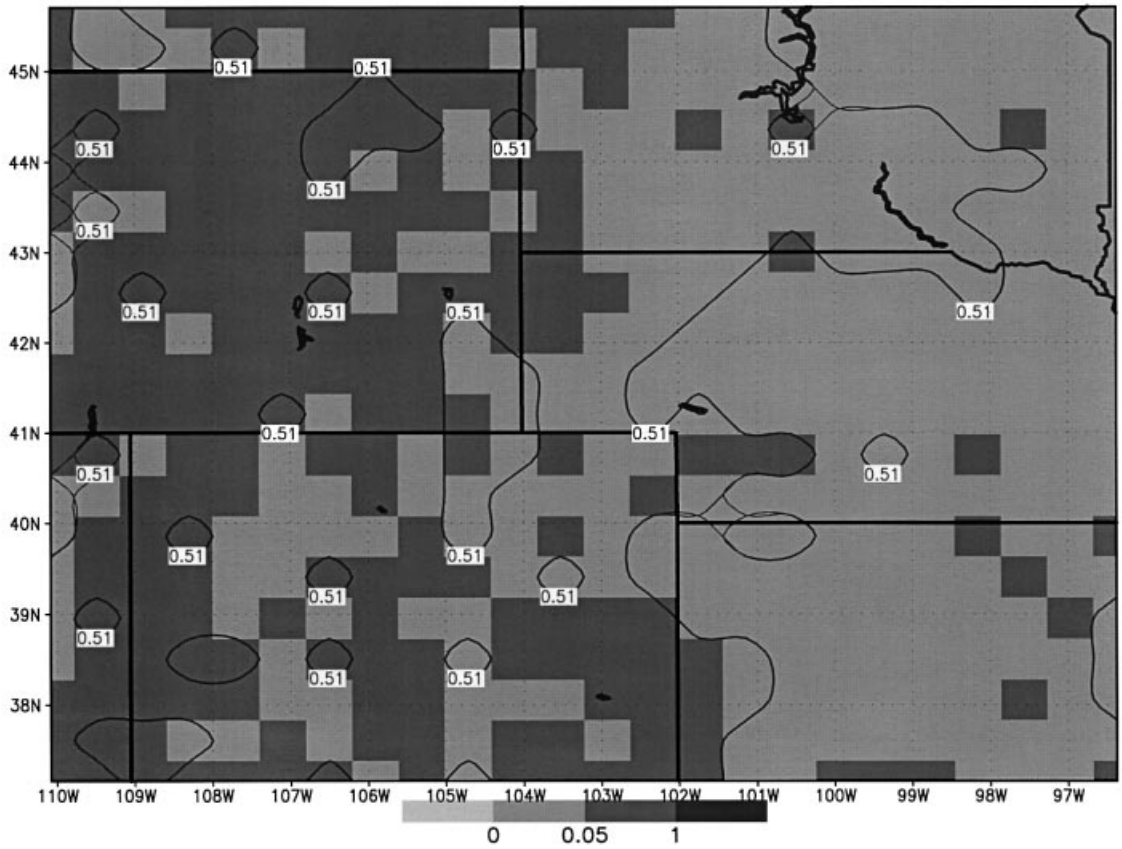

Fig. 11 KS test for shoot biomass. The lighter grey areas indicate no significance while the darker grey areas represent significant differences at $\alpha = 0.05$. The contour lines denote the boundary between altered and unaltered vegetation.

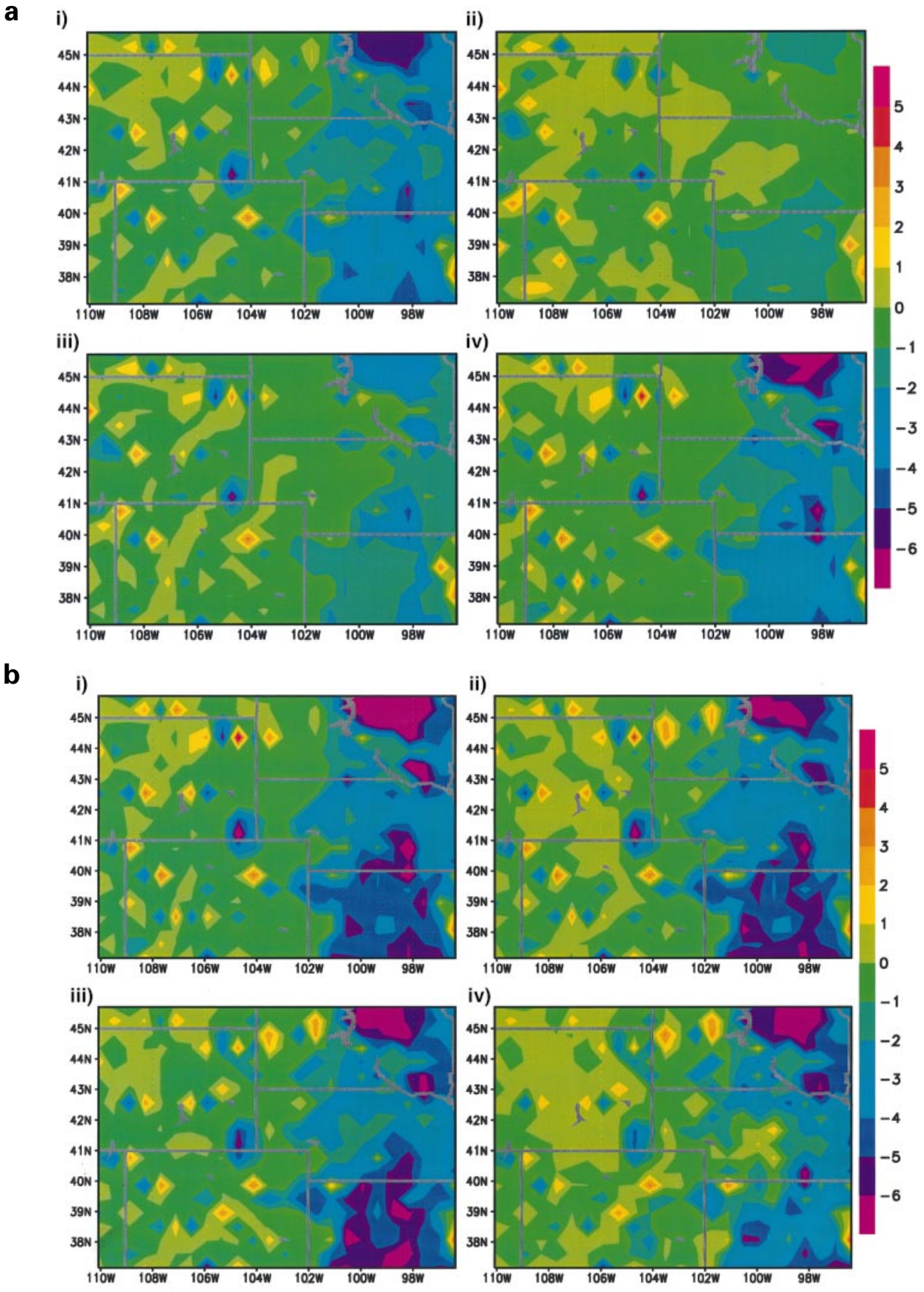
a
i)
ii)
iii)
iv)
45N
44N
43N
42N
41N
40N
39N
38N
110W
108W
106W
104W
102W
100W
98W
5
4
3
2
1
0
−1
−2
−3
−4
−5
−6
b
i)
ii)
iii)
iv)

current vegetation simulation was integrated with $2 \times CO_2$ radiation and $2 \times CO_2$ biology. The seasonal average displayed in 13a(i) is considerably different from that displayed in Fig. 12a. The spatial plot indicates that nearly the entire western half of the domain is experiencing cooling effects resulting from the combination of current vegetation and $2 \times CO_2$ radiation and biology. Some areas are cooler by nearly 4 °C, with large portions roughly half this magnitude. The results shown in this the figure also demonstrate that the effects owing to landscape change have been reduced over agricultural areas. The plots for April to June also show substantial differences from the $1 \times CO_2$ counterparts. Notice that in April the western portion of the domain does not exhibit a general cooling trend; in May and June, however, the signal switches to cooling over much of the west. During this 3-month period, the eastern agricultural areas are similar under both $1\times$ and $2 \times CO_2$, as would be expected as the agricultural areas are not near their peak maturity.

The final four months of the analysis are displayed in Fig. 13(b). As was shown in the previous figure, the eastern portion of the domain shows a strong warming signal, although it has been reduced compared to the $1 \times CO_2$ results. What is most obvious is the strong cooling that appears in the north central portions of the domain, reaching nearly 5 °C in magnitude. Overall, the cooling extends past the foothills into the eastern plains, unlike the $1 \times CO_2$ results that indicated the cooling was largely confined to patches in the mountains.

The model's sensitivity indicates that the combination of landscape change and $2 \times CO_2$ biology contribute significantly to the prognosed maximum temperature field, and as seen in the analysis throughout this paper, to many other meteorological and biological variables. The model also suggests that doubling CO_2 on regional and seasonal scales could lead to cooling over substantial areas, and reduce the heating effects over the agricultural areas.

Summary and conclusions

The validation portion of this paper has demonstrated the ability of a mechanistic coupled plant and meteorological modelling system to represent a growing season in terms of temperature, moisture, and biomass fields. This was demonstrated on a domain-averaged basis and over individual gridpoints. The skill of the model was strongest for temperature and biomass fields, and exhibited a weakness in representing the magnitude of the precipitation. However, the temporal results of the precipitation demonstrated good agreement.

The results from this study indicate significant differences for biological and meteorological variables in domain-averaged, diurnal, and gridpoint means and cumulative distributions due to individual factors, which include landscape change, $2 \times CO_2$ radiation, and $2 \times CO_2$ biology.

Several proposed mechanisms for these differences where pointed out. In general, changing the underlying biome characteristics – whether the result of a complete biome replacement, or of enhanced biomass through elevated CO_2 – will alter the surface energy budget through albedo changes and the partitioning of latent and sensible heat fluxes.

A change in albedo will alter the absorption and reflection solar radiation. A modified albedo can result from all of the factors investigated, although it is obvious that the $2 \times CO_2$ radiation impact would be minimal as it is addressed in this study.

In the case of landscape change, the albedo can change spatially as well as temporally. For example, the conversion from grassland to cropland has both changes. During the early growing season the albedo of a cropping system is much lower than grassland at the same point in the season, especially senescent grassland (this modelling system does account for the seasonal albedo change in the grassland). As the growing season progresses, and the crops near maturity, the differences in albedo will not be as significant between the two biome types. Finally, harvest occurs in the current landscape and again a dramatic difference in albedo is realized between the two landscape types. Simultaneously, these differences in shortwave partitioning are involved in altering local temperature and moisture fields. Figure 12(a,b) clearly demonstrate this temporal and spatial response.

The evolution of albedo in the case of $2 \times CO_2$ biology with no landscape change, results from biomass increases leading to a higher fractional coverage by vegetation, which reduces the exposure of the soil. In closed canopy systems, such as the western forests, this effect is minimized because the soil is already covered. The cooling signal (not shown) was clearly strongest over the eastern plains and was found to be minimal in western forested areas. The enhanced fractional coverage

Fig. 12 (a) Monthly-averaged maximum daily temperature (°C) for natural minus current vegetation simulations conducted at $1 \times CO_2$ for radiation and biology. (i) Seasonal average, (ii) April, (iii) May, and (iv) June. (b) Monthly-averaged maximum daily temperature (°C) for natural minus current vegetation simulations for (i) July, (ii) August, (iii) September, and (iv) October.

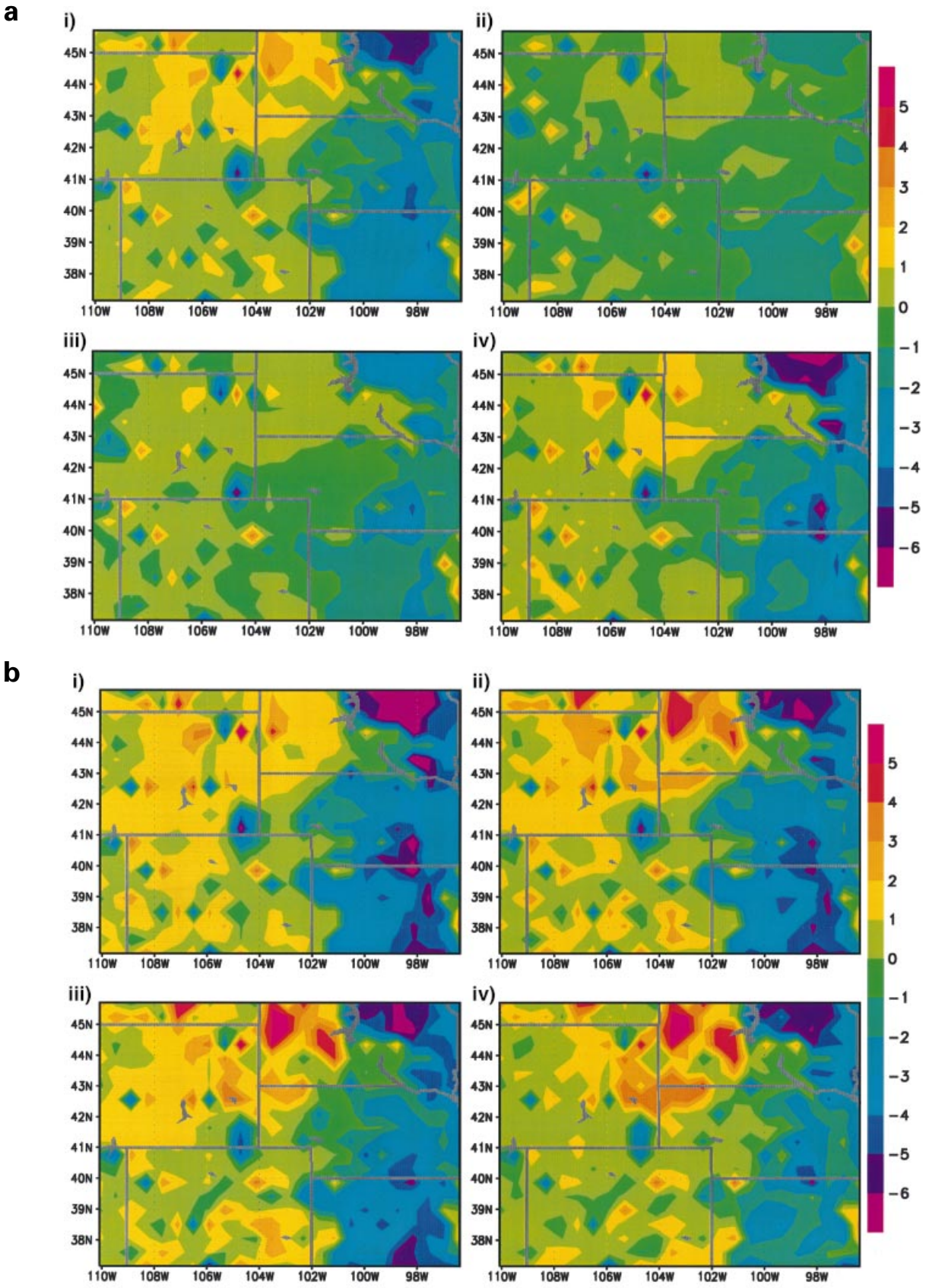
a
i)
ii)
iii)
iv)
45N
44N
43N
42N
41N
40N
39N
38N
110W
108W
106W
104W
102W
100W
98W
5
4
3
2
1
0
−1
−2
−3
−4
−5
−6
b
i)
ii)
iii)
iv)

in the grasslands will decrease the evaporation from the soil, and allow more water to be available to the plants, which will further promote transpirational cooling.

The available water is also important in the partitioning of latent and sensible heat fluxes. How the vegetation partitions these fluxes is again influenced most strongly by $2 \times CO_2$ biology and landscape change. Returning to the crop versus grassland example, there is a strong seasonal influence on the latent to sensible heat ratio (Bowen ratio). In the case of the crops, the barren fields will exhibit a different Bowen ratio from that of the grassland early in the growing season. As shown in Fig. 12(b), the cooling signal in eastern plains is not nearly as strong, indicating that the evaporation is larger when bare fields are saturated earlier in the year. During early summer months the LAI of the croplands is less than the corresponding grasslands, which leads to larger sensible heat flux and higher daytime temperatures. It was also seen that when the $2 \times CO_2$ biology treatment was applied to the current landscape (Fig. 13a,b) the maximum daily temperature differences between the current and natural landscapes were reduced, which implies a higher latent heat flux.

It was also shown that a biological teleconnection was found in the analysis of land-use change. This is a consequence of the communication of heat, momentum, and moisture through advection and diffusion. The most obvious mechanism producing these changes can be attributed to spatial variations in the surface heat flux and to the aerodynamic roughness of the surface. These variations will clearly modify advection patterns and the mixing characteristics of the boundary layer. For example, a bare field will have a significantly different heat flux and roughness length than that of grassland. The partitioning of sensible and latent heat, clearly different for dissimilar landscape types is found to be relevant in our study in assessing regional impacts of human land change, and was also found on a global scale in studies by Chase *et al*. (1996, 2000). Given the results of Vitousek *et al*. (1997), suggesting that human impact has altered about 45% of the land surface of the Earth, this model's sensitivity implies that regional-scale impacts on weather following land-use change will occur at numerous locations.

Factor interactions were found to contribute to the total field, although they were generally smaller in magnitude than individual factor contributions. However, the analysis presented here was limited to a few variables. Results not shown here demonstrate a magnitude of factor interaction similar to individual factor contributions on individual gridpoints. In the case of the factor interaction of $2 \times CO_2$ with natural vegetation, for example, the results showed a magnitude similar to that of the $2 \times CO_2$ radiation factor contribution (Fig. 8).

Finally, the model results suggest that the $2 \times CO_2$ biological effect can dominate the overall effects on temperature. This must be interpreted in the context it was presented. This is a regional-scale sensitivity study. These results cannot be linearly scaled up to global scales. In a global context they do, however, suggest that the regional response could be on the order of global climate sensitivities. As pointed out in the introduction, the role of down-regulation also needs to be addressed. At this time, the present authors are implementing a soil organic model in order to capture some of the effects of nitrogen deficiency. Other experiments are being conducted limiting the enhancement of photosynthesis rates owing to CO_2 enrichment. Still, the model's sensitivity indicates that doubling of CO_2 should be accounted for in a mechanistic interactive way in order to begin to properly quantify its impact. Indeed, climate change that results from anthropogenic increases of CO_2 must consider the biological effects of enriched CO_2 as well as its radiative effect. Overall, this paper outlined a technique that begins to dissect the complicated problem of biological and atmospheric interactions resulting from various factors and their interactions.

Acknowledgements

Acknowledgements are extended to the institutions that provided the necessary support to complete this work. These include NASA Grant No. NAG8-1511, NSF Grant No. ATM-9910857, EPA Grant No. R824993-01–0, Tulane University Contract No. TUL-062–98/99, and NSF Grant No. DEB-9524129.

References

Anderson TW, Darling DA (1952) Asymptomatic theory of certain 'goodness of fit' criteria based on stochastic processes. *Annals of Mathematical Statistics*, **23**, 193–212.

Asrar G, Fuchs M, Kanemasu ET, Hatfield JL (1984) Estimating absorbed photosynthetic radiation and leaf area index from spectral reflectance in wheat. *Agronomical Journal*, **76**, 300–306.

Avissar R (1995) Recent advances in the representation of land–atmosphere interactions in general circulation models. In: *U.S. National Report to International Union of Geodesy and Geophysics 1991–94. Reviews of Geophysics*, Suppl., 1005–1010.

Ball JT, Woodrow IE, Berry NA (1987) A model predicting

Fig. 13 (a) Monthly-averaged maximum daily temperature (°C) for natural minus current vegetation simulations. The current vegetation simulations were conducted at $2 \times CO_2$ for radiation and biology, while the natural simulation used $1 \times CO_2$ for radiation and biology. (i) Seasonal average (ii) April, (iii) May, and (iv) June. (b) Monthly-averaged maximum daily temperature (°C) for natural minus current vegetation simulations for (i) July, (ii) August, (iii) September, and (iv) October.

stomatal conductance and its contribution to the control of photosynthesis under different environmental conditions. In: *Progress in Photosynthesis Research* (ed. Biggins I), **Vol. IV**, pp. 221–224. Martinees Nijhof, Dordrecht.

Bazzaz FA (1990) The response of natural ecosystems to the rising global CO_2 levels. *Annual Review of Ecological Systems*, **21**, 167–196.

Bazzaz FA, Williams WE (1991) Atmospheric CO_2 concentrations within a mixed forest: implications for seedling growth. *Ecology*, **72**, 12–16.

Betts RA, Cox PM, Lee SE, Woodward FI (1997) Contrasting physiological and structural vegetation feedbacks in climate simulations. *Nature*, **387**, 796–799.

Bonan GB, Pollard D, Thompson SL (1992) Effects of boreal forest vegetation on global climate. *Nature*, **359**, 716–718.

Brostrom A, Coe M, Harrison SP *et al.* (1998) Land surface feedback and paleomonsoons in northern Africa. *Geophysical Research Letters*, **25**, 3615–3618.

Bryant J, Taylor G, Frehner M (1998) Photosynthetic acclimation to elevated CO_2 is modified by source: sink balance in three component species of chalk grassland swards grown in a free air carbon dioxide enrichment (FACE) experiment. *Plant, Cell and Environment*, **21**, 159–168.

Chase TN, Pielke RA, Kittel TGF, Nemani R, Running SW (1996) The sensitivity of a general circulation model to global changes in leaf area index. *Journal of Geophysical Research*, **101**, 7393–7408.

Chase TN, Pielke RA Sr, Kittel TGF, Nemani RR, Running SW (2000) Simulated impacts of historical land cover changes on global climate in northern winter. *Climate Dynamics*, **16**, 93–105.

Chen J (1983) The reciprocity relation for reflection and transmission of radiation by crops and other plane-parallel scattering media. *Remote Sensing Environment*, **13**, 475–486.

Chen D-X, Coughenour MB (1994) GEMTM: a general model for energy and mass transfer of land surfaces and its application at the FIFE sites. *Agriculture and Forest Meteorology*, **68**, 145–171.

Chen D-X, Lieth JH (1992) Two-dimensional model of water transport in the rootzone and plant for container-grown chrysanthemum. *Agriculture and Forest Meteorology*, **59**, 129–148.

Chen D-X, Lieth JH (1993) A two-dimensional, dynamic model for root growth distribution of potted plants. *Journal of the American Society of Horticultural Science*, **118**(2), 181–187.

Chen D-X, Coughenour MB, Knapp AK, Owensby CE (1994) Mathematical simulation of C_4 grass photosynthesis in ambient and elevated CO_2. *Ecological Modeling*, **73**, 63–80.

Claussen M (1994) On coupling global biome models with climate models. *Climate Research*, **4**, 203–221.

Claussen M (1998) On multiple solutions of the atmosphere-vegetation system in present-day climate. *Global Change Biology*, **49**, 2212–2262.

Claussen M, Gaylor V (1997) The greening of Sahara during the mid-Holocene: results of an interactive atmosphere – biome model. *Global Ecology and Biogeography Letters*, **6**, 369–377.

Collatz GJ, Ribas-Carbo M, Berry JA (1992) Coupled photosynthesis-stomatal conductance model for leaves of C_4 plants. *Australian Journal of Plant Physiology*, **19**, 519–538.

Cotton WR, Weaver JF, Beitler BA (1995) An unusual summertime downslope wind event in Fort Collins, Colorado, on 3 July, 1993. *Weather and Forecasting*, **10**, 786–797.

Crowley TJ, Baum SK (1997) Effect of vegetation on an ice-age climate model simulation. *Journal of Geophysical Research*, **102**(D14), 16,463–14,680.

Cutrim ED, Martin W, Rabin R (1995) Enhancement of cumulus clouds over deforested lands in Amazonia. *Bulletin of the American Meteorological Society*, **76**, 1801–1805.

De Noblet N, Prentice IC, Jousaume S, Texier D, Botta A, Haxeltine A (1996) Possible role of atmosphere–biosphere interactions in triggering the last glaciation. *Geophysical Research Letters*, **23**, 3191–3194.

De Ridder K, Gallee H (1998) Land surface-induced regional climate change in southern Israel. *Journal of Applied Meteorology*, **37**, 1470–1488.

Dirmeyer PA, Shukla J (1994) Albedo as a modulator of climate response to tropical deforestation. *Journal of Geophysical Research*, **99**, 20,863–20,877.

Eamus D (1996) Responses of field grown trees to CO_2 enrichment. *Commonwealth Forestry Review*, **75**, 39–47.

Eastman JL (1999) Analysis of the effects of CO_2 and landscape change using a coupled plant and meteorological model. PhD Dissertation, Department of Atmospheric Science, Colorado State University.

Farquhar GD, von Caemmerer S, Berry JA (1980) A biochemical model of photosynthetic CO_2 assimilation in leaves of C_3 species. *Planta*, **149**, 78–90.

Foley JA (1994) The sensitivity of the terrestrial biosphere to climate change: a simulation of the middle Holocene. *Global Biogeochemical Cycles*, **8**, 505–525.

Foley JA, Levis S, Prentice IC, Pollard D, Thompson SL (1998) Coupling dynamic models of climate and vegetation. *Global Change Biology*, **4**, 561–580.

Ganopolski A, Kubatzki C, Claussen M, Brovkin V, Petoukhov V (1998) The role of vegetation–atmosphere–ocean interaction for the climate system during the midHolocene. *Science*, **280**, 1916–1919.

Goudriaan J (1977) *Crop Micrometeorology: a simulation study.* Center for Agricultural Publishing and Documentation, Wageningen.

Idso SB (1992) Shrubland expansion in the American Southwest. *Journal of Climate Change*, **22**, 85–86.

Kalnay EM, Kanamitsu R, Kistler W *et al.* (1996) The NCEP/NCAR 40-year reanalysis project. *Bulletin of the American Meteorological Society*, **77**, 437–471.

Kanae S, Oki T, Musiake K (1999) Game-tropics studies on deforestation effects in Indochina. *GEWEX News*, **9**(1), 4.

Kiang JE, Eltahir EAB (1999) Role of ecosystem dynamics in biosphere–atmosphere interaction over the coastal region of West Africa. *Journal of Geophysical Research*, **104**, 31,173–31,189.

Kittel TGF, Rosenbloom NA, Painter TH, Schimel DS, *VEMAP Modeling Participants* (1995) The VEMAP integrated database for modeling United States ecosystem/vegetation sensitivity to climate change. *Journal of Biogeochemical Cycling*, **22**, 857–862.

Küchler AW (1964) *Potential Natural Vegetation of the Conterminous United States*. Special Publication No. 36. American Geophysical Society.

Küchler AW (1975). *Potential Natural Vegetation of the United States*, 2nd edn. (Map scale 1: 3,168,000.) American Geographical Society, New York.

Kuo HL, Raymond WH (1980) A quasi-one-dimensional cumulus cloud model and parameterization of cumulus heating and mixing effects. *Monthly Weather Review*, **101**, 547–553.

Li D, Komiyama H, Kurihara K, Sata Y (2000) Case studies of the impact of landscape changes on weather modification in western Australia in summer. *Journal of Geophysical Research*, **105**, 12,303–12,315.

Liston GE, Pielke RA (2000) A climate version of the Regional Atmospheric Modeling System. *Theoretical and Applied Climatology*, **66**, 29–47.

Lyons TJ, Schwerdtfeger P, Hacker JM, Foster IJ, Smith RCG, Xinmei H (1993) Land–atmosphere interaction in a semiarid region: The bunny fence experiment. *Bulletin of the American Meteorological Society*, **74**, 1327–1334.

Mahrer Y, Pielke RA (1977) A numerical study of the airflow over irregular terrain. *Beitrage Zur Physik der Atmosphäre*, **50**, 98–113.

Mintz Y, Serafini Y (1981) Global Fields of Soil Moisture and Land-Surface Evapotranspiration. Technical Memorandum 83907. *NASA Goddard Space Flight Center Research Review*, **1980/81**, 178–180.

Nemani R, Running SW (1989) Testing a theoretical climate-soil-leaf area hydrologic equilibrium of forests using satellite data and ecosystem simulation. *Agricultural and Forest Meteorology*, **44**, 245–260.

O'Brien K (2000) Upscaling tropical deforestation: Implications for climate change. *Climatic Change*, **44**, 311–329.

Owensby CE (1993) Potential impacts of elevated CO_2 and above- and belowground litter quality of a tallgrass prairie. *Water, Air, and Soil Pollution*, **70**, 413–424.

Pielke RA (1998) Climate prediction as an initial value problem. *Bulletin of the American Meteorological Society*, **79**, 2743–2746.

Pielke RA (2001) Influence of the spatial distribution of vegetation and soils on the prediction of cumulus convective rainfall. *Review of Geophysics*, **39**, 151–177.

Pielke RA Sr, Liston GE, Eastman JL, Lu L, Coughenour MB (1999) Seasonal weather prediction as an initial value problem. *Journal of Geophysical Research*, **104**, 19,463–19,479.

Reynolds JF, Acock B (1985) Predicting the response of plants to increasing carbon dioxide: a critique of plant growth models. *Ecological Modeling*, **29**, 107–129.

Ryan MG (1991) Effects of climate change on plant respiration. *Ecological Applications*, **1**, 157–167.

Ryan MG, Lavigne MB, Gower ST (1997) Annual carbon cost of autotrophic respiration in boreal forest ecosystems in relation to species and climate. *Journal of Geophysical Research*, **102**, 28871–28883.

Sellers PJ, Dickinson RE, Randall DA *et al.* (1997) Modeling the exchanges of energy, water, and carbon between continents and the atmosphere. *Science*, **275**, 502–509.

Sivillo JK, Ahlquist JE, Toth Z (1997) An ensemble forecasting primer. *Weather and Forecasting*, **12**, 809–818.

Stein U, Alpert P (1993) Factor separation in numerical simulations. *Journal of Atmospheric Science*, **50**, 2107–2115.

Texier D, de Noblet N, Harrison SP *et al.* (1997) Quantifying the role of biosphere atmosphere feedbacks in climate change: Coupled model simulations for 6000 years BP and comparison with paleodata for northern Eurasia and northern Africa. *Climate Dynamics*, **13**, 865–882.

Tremback CJ, Kessler R (1985) A surface temperature and moisture parameterization for use in mesoscale numerical models. Preprints. In: *7th Conference on Numerical Weather Prediction, 17–20 June, 1985, Montreal, Canada*, AMS.

U.S. Department of Agriculture (1994) *State Soil Geographic (STATSGO) Data Base—Data Use Information* (rev. ed.). Miscellaneous Publication of the Number 1492. Natural Resources Conservation Service, Fort Worth, TX.

Vitousek PM, Mooney HA, Lubchenco J, Melillo JM (1997) Human domination of earth ecosystems. *Science*, **277**, 494–499.

Wang G, Eltahir EAB (2000a) Role of vegetation dynamics in enhancing the low frequency variability of the Sahel rainfall. *Water Resources Research*, **36**, 1013–1021.

Wang G, Eltahir EAB (2000b) Ecosystem dynamics and the Sahel drought. *Geophysical Research Letters*, **27**, 795–798.

Wang G, Eltahir EAB (2000c) Biosphere–atmosphere interactions over West Africa. I: Development and validation of a coupled dynamic model. *Quarterly Journal of the Royal Meteorological Society*, **126**, 1239–1260.

Wang G, Eltahir EAB (2000d) Biosphere–atmosphere interactions over West Africa, II: Multiple climate equilibria. *Quarterly Journal of the Royal Meteorological Society*, **126**, 1261–1280.

Wang G, Bras RL, Eltahir EAB (2000) The impact of observed deforestation on the mesoscale distribution of rainfall and clouds in Amazonia. *Journal of Hydrometeorology*, **1**, 267–286.